Measurements of the K-Shell Opacity of a Solid-Density Magnesium Plasma Heated by an X-Ray Free-Electron Laser

T. R. Preston, S. M. Vinko, O. Ciricosta, P. Hollebon, H.-K. Chung, G. L. Dakovski, J. Krzywinski, M. Minitti, T. Burian, J. Chalupský, V. Hájková, L. Juha, V. Vozda, U. Zastrau, R. W. Lee, and J. S. Wark

Phys. Rev. Lett. **119**, 085001 — Published 25 August 2017

DOI: 10.1103/PhysRevLett.119.085001

Measurements of the K-shell Opacity of a Solid-Density Magnesium Plasma Heated by an X-ray Free Electron Laser

T. R. Preston,[1] S. M. Vinko,[1] O. Ciricosta,[1] P. Hollebon,[1] H.-K. Chung,[2]
G. L. Dakovski,[3] J. Krzywinski,[3] M. Minitti,[3] T. Burian,[4] J. Chalupský,[4]
V. Hájková,[4] L. Juha,[4] V. Vozda,[4] U. Zastrau,[5] R. W. Lee,[6] and J. S. Wark[1,*]

[1]*Department of Physics, Clarendon Laboratory, University of Oxford, Parks Road, Oxford OX1 3PU, United Kingdom*
[2]*Atomic and Molecular Data Unit, Nuclear Data Section, IAEA, P.O. Box 100, A-1400 Vienna, Austria*
[3]*SLAC National Accelerator Laboratory, 2575 Sand Hill Road, Menlo Park, CA 94025, USA*
[4]*Institute of Physics ASCR, Na Slovance 2, 18221 Prague 8, Czech Republic*
[5]*European XFEL GmbH, Holzkoppel 4, 22869 Schenefeld, Germany*
[6]*Department of Physics, University of California, Berkeley, California 94720, USA*

(Dated: June 21, 2017)

We present measurements of the spectrally-resolved X-rays emitted from solid-density magnesium targets of varying sub-μm thicknesses isochorically heated by an X-ray laser. The data exhibit a largely thickness-independent source function, allowing the extraction of a measure of the opacity to K-shell X-rays within well-defined regimes of electron density and temperature, extremely close to local thermodynamic equilibrium (LTE) conditions. The deduced opacities at the peak of the K-α transitions of the ions are consistent with those predicted by detailed atomic-kinetics calculations.

The generation of uniformly dense and uniformly-heated high-density plasmas created sufficiently rapidly so as to prevent significant hydrodynamic motion during their diagnosis has long been a goal in the field of laser-matter interactions, as such plasmas would provide an environment to make benchmark tests of several fundamental optical, thermodynamic and transport properties of strongly coupled matter which are important for furthering our understanding of systems relevant to astrophysics [1], planetary science [2], and inertial confinement fusion [3, 4]. Whilst heating matter with electrons [5–7] or ions [8–10] driven by short-pulse optical light has afforded significant progress in this area, it is with the advent of Free Electron Lasers (FELs) operating in the X-ray regime, such as the Linac Coherent Light Source (LCLS) [11], that the capability to create hot plasmas at exactly solid densities has been conclusively demonstrated, with the relatively long absorption depths of X-rays and absence of pre-pulse allowing micron-scale matter to be heated on femtosecond timescales with negligible longitudinal temperature variation [12–14].

Previous studies of such plasmas have shown that, owing to the high electron densities and thus large collisional rates [15], the systems are extremely close to LTE, with the populations of the majority of the atomic states being determined by the instantaneous electron temperature [16]. More precisely, for low-to-medium Z materials such as magnesium studied here, whilst the ground state populations are mainly determined by the collisional physics, and are thus in LTE, during the FEL pulse at any instant a few percent of the ions have a K-shell core-hole induced by the intense FEL photoionization, and in this restricted sense this small number of atoms is driven out of LTE. However, any reabsorption of the K-α photons emitted from the filling of these K-shell holes is mainly due to bound-bound transitions originating from a ground state ion (the one corresponding to the final state of the K-α transition), so that measuring the opacity of these K-α lines is essentially a measurement of LTE opacity.

As the absorption length of the system to the heating X-ray beam is long our system is relatively free of longitudinal gradients and the ionic populations are independent of target thickness d along the X-ray beam direction. Therefore, if the transverse scale-lengths are long compared with the target thickness, the instantaneous frequency-dependent intensity $I(\nu, t, d, \theta)$ emitted at an angle θ to the normal of a target of thickness d owing to the filling of these core holes obeys the simple, 1D uniform slab solution to the equation of radiative transfer,

$$I(\nu, t, d, \theta) = S(\nu, t)[1 - \exp(-\kappa(\nu, t)d/\cos\theta)], \quad (1)$$

where the source function, $S(\nu, t)$, is given by the ratio of the emissivity to the opacity, both uniform in depth: $S(\nu, t) = \eta(\nu, t)/\kappa(\nu, t)$. The emissivity (and hence source function) is determined by the number of FEL-induced core holes.

Despite the simplicity of this well-known equation, to our knowledge no experimental demonstration of its direct application for a very dense plasma has previously been reported. This is for a number of reasons. Firstly, it is non-trivial to produce 'slabs' of plasmas, of differing thickness but otherwise identical, where the effects of longitudinal density and temperature gradients are unimportant. Secondly, in many cases, laser-driven plasmas suffer from the effects of self-absorption which affects their atomic-kinetics and the populations of the ground states, as well as the excited states (an effect that is often taken into account in simple treatments via an escape

factor formalism [17, 18]). In our case this is negligible: the intense FEL drives the population kinetics, and rapid collisional rates ensure our ground state populations are set by LTE [19] – in other words, the emissivity $\eta(\nu, t)$ and opacity $\kappa(\nu, t)$ are a weak function of thickness d. Finally, verifying the applicability of Eqn. 1 requires observing emission in both the optically thick ($\kappa(\nu, t)d > 1$) and thin ($\kappa(\nu, t)d \ll 1$) regimes, the latter requiring extremely thin targets at solid density – for the work here just a few tens of nm – again necessitating rapid heating with no pre-pulse and diagnosis on the sub-picosecond timescale of inertial confinement.

It is in this context that we present here spectrally-resolved measurements of the X-ray emission from thin foils of solid magnesium heated with an X-ray FEL to peak electron temperatures of order 180 eV by the end of the pulse. We show that the time-integrated FEL-induced K-shell emission from the various ion stages up to helium-like Mg obeys well the same functional form as Eqn. 1. We determine frequency-resolved opacities from this thickness-dependent emission which, whilst extracted from time-integrated emission from a plasma whose temperature and charge states are varying in time, can be shown to be a good measure of the maximum opacity present within the system for the majority of the charge states. Given that the ion density remains that of the solid, the electron densities at which these measurements are gleaned is strongly constrained. The derived opacities are in good agreement with atomic-kinetics calculations.

The experiment was performed at the SXR endstation [20] of LCLS. Targets comprising thin (24 nm - 487 nm ± 2 nm) foils of Mg were irradiated by ∼ 50 fs pulses of X-rays (shorter than the nominal electron bunch duration, consistent with previous work [16, 21–23]), with a photon energy of 1540 eV, and nominal pulse energy of 1.8 mJ prior to transmission through the beamline focussing optics, which was estimated from the mirror reflectivities to be ∼50% [16]. The target was oriented at an angle of 45° to the incident X-ray beam. The spatial distribution of X-ray intensities on target was determined *ex situ* via imprint measurements in PbI_2 [24], and the focal spot on target had an effective area of 8.5 μm^2, corresponding to a peak irradiance around 10^{17} Wcm^{-2}. At these irradiances simulations show the electrons within the target are heated to a peak temperature of order 180 eV by the end of the pulse. The primary absorption mechanism is direct photoionization, resulting in the creation of K-shell holes. The majority of these K-shell holes are filled as a result of the KLL Auger decay (the electrons from which rapidly thermalise [15, 25]), with approximately 3% of them filled by radiative decay from the L to K shell. These radiative transitions were recorded by means of a flat crystal Bragg spectrometer which employed a Beryl ($10\bar{1}0$) crystal ($2d$ = 15.96 Å), with the spectrometer viewing the target at an angle θ of 20° to its normal, recording X-rays on a Princeton Instruments CCD camera.

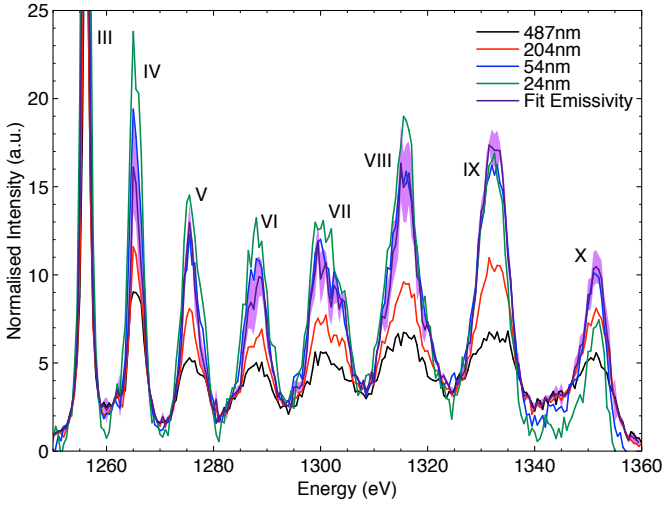

FIG. 1. Experimental X-ray emission spectra for Mg targets of four different thicknesses, heated by the LCLS X-ray pulse. Each spectrum is the average of spectra from multiple shots, normalised by the target thickness. The lines are labelled according to the charge state of the emitting ion. Also shown is the emissivity extracted by fitting Eqn. 1 to the four experimental spectra. The coloured region around the fitted emissivity represents its error bar.

Although Eqn. 1 is only valid for a uniform plasma, the line of sight just described is such that the maximum displacement between incoming and outgoing photons on the plane of the laser is well within the Half-Width-Half-Maximum of the beam profile, even for the thickest target, thus ensuring approximately uniform conditions in the region where radiation transfer occurs. However, within our detailed analysis such geometric effects are taken into account (see supplemental material) and have the largest effect on the higher lying lines, for which the corresponding charge states are only produced towards the central region of the focal spot containing the highest X-ray energy density.

In Fig. 1 we plot the time-integrated emission summed over many (between 10 and 123) distinct single shots normalised both to the number of shots and to d for the four different target thicknesses. For each thickness, the figure shows the series of K-α emission lines corresponding to transitions of L electrons filling K-shell holes, created by the LCLS photons, in ions with a different number of L-shell holes, labelled by their charge state (noting cold solid density Mg already has 2 free electrons, and the cold K-α comes from charge state III). As in previous experiments [12, 13, 16] the temperatures attained are too low for the targets to emit thermally on such transitions, and the line spectra recorded thus correspond to radiation that is only emitted during the short duration of the FEL pulse itself convolved with the lifetime of the

K-shell core-hole state (which is dominated by Auger decay, and is typically of order 3 fs for most states, save the helium-like state which has no Auger channel), and are thus a probe of the target under truly isochoric conditions, which further allows the electron density during the emission from a particular charge state to be deduced from the ion stage.

The signature of emission in the optically-thin limit is that the intensity normalised to target thickness is independent of d, because if $\kappa(\nu,t)d/\cos\theta \ll 1$ throughout the pulse, then $\int I(\nu,t,d,\theta)[\cos\theta/d]\mathrm{d}t \rightarrow \int \eta(\nu,t)\mathrm{d}t$ — the same for each target. It can be seen from Fig. 1 that the emission from 24 and 54 nm targets is in the optically thin limit across the whole spectral range, whilst for the two thicker targets opacity effects are evident at the peaks of the K-α emission from each ion, but the emission is still optically thin in the far wings of the transitions, i.e. the region between the K-α lines.

Assuming for the present (with a justification below) that the time-integrated intensity $\int I(\nu,t,d,\theta)\mathrm{d}t$ is well approximated by an equation of the form of Eqn. 1, we can fit Eqn. 1 to the time-integrated emission from the four targets for any photon energy within the spectral range of the spectrometer. As examples in Fig. 2a we show such fits for the frequencies corresponding to the centre of the Be-like K-α (VIII) line at 1315eV, and to the line wings between the Be-like and Li-like K-α lines at 1325eV. As the opacity for the line wing is low, the fit approaches a linear trend in this case (given by the optically thin limit of Eqn. 1), whereas the line centre has a larger opacity, and here the intensity begins to saturate at larger thicknesses. By performing such a fit over the whole recorded spectral range, we obtain the frequency-dependent values of the effective emissivity and opacity, $\kappa(\nu)$, shown in in Fig. 2b.

We stress that the opacities plotted in Fig. 2b are not those of a plasma at an exact density and temperature, as they have been deduced from time and space-integrated emission data from a system that evolves over time. As the system is heated by the FEL the population of each charge state and set of configurations - whether they correspond to emitters or absorbers - will change, as will the emissivity and opacity at a particular frequency. However, as we show below, each charge state only exists over a relatively narrow range of temperatures and densities, and as these are swept through the resultant integrated emission for targets of different thicknesses closely follows Eqn. 1, with an 'integrated opacity' which is a good measure of the maximum LTE opacity for any particular photon energy.

To illustrate this, the experimental data were simulated using the collisional-radiative code SCFLY [26] which has previously been shown to produce excellent agreement with spectra produced by LCLS interacting with solid targets [16]. Simulations over a range of FEL intensities calculate the local time-dependent populations of super-configurations within the target, with the only user input being the time-dependent incident X-ray pulse. At each time-step a spectrum taking into account the more detailed configurational energies is produced, with an instantaneous thickness-dependent intensity that obeys Eqn. 1. Appropriate weighting of the time-integrated spectra from the simulations according to the experimentally measured spatial distribution of the FEL intensities within the focal spot allows direct comparison with experimental data. Further to this, spectra

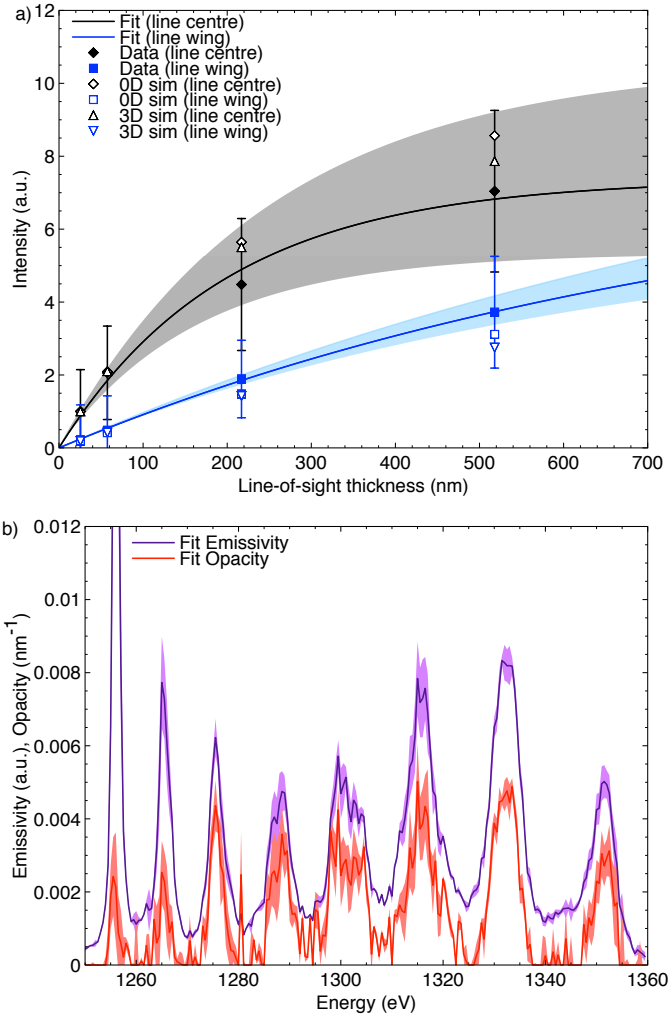

FIG. 2. (a) Filled symbols: intensity as a function of line of sight thickness, $d/\cos\theta$, at the centre of line VIII (1315 eV) and between peaks in the line wings (1325 eV) for the four different target thicknesses. Open symbols: intensity predicted by SCFLY simulations for 0D simulations or a full 3D model of the target including geometric effects. The solid line is the fit to the radiative transfer equation for data at 1315 eV (black), and and the dashed line is the fit at 1325 eV (blue). (b) Opacity and emissivity as a function of photon energy deduced by fitting Eqn. 1 to the spectra from targets of four different thicknesses. The solid region represents the calculated error in the fit.

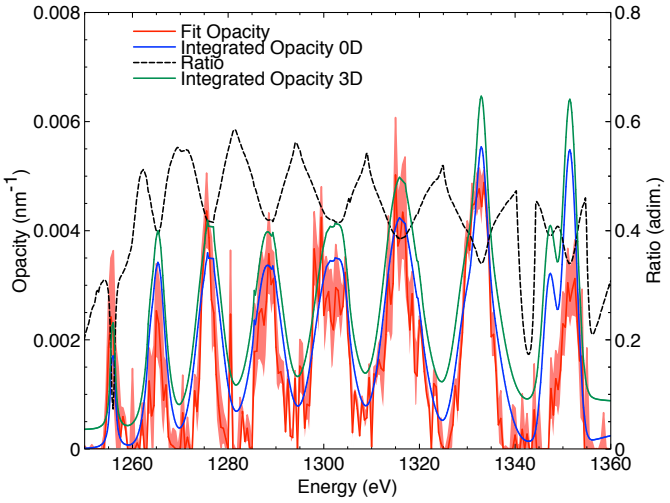

FIG. 3. A comparison between the 'integrated opacity' deduced from the data and that deduced from the time and space-integrated spectra produced from 0D SCFLY simulations, and 3D SCFLY simulations. Also plotted, for each frequency, is the ratio of 'integrated opacity' observed in the 0D simulation to the maximum instantaneous opacity.

were calculated incorporating a full 3D model accounting for the different heating and line-of-sight directions, and attenuation through the target [19].

From the SCFLY simulations we generate time- and space-integrated frequency-dependent intensities for targets of the four different thicknesses that are a good match to the data within the error bars, as shown in Fig. 2a for both a simple 0D model and the 3D model. Whilst, by construction, an instantaneous set of simulated intensities for the four different targets matches perfectly Eqn. 1, the fact that the simulated time and space-integrated data correctly reproduce the form shown in Fig. 2a also yields the non-trivial result that the same functional form is a good match to the time-integrated simulated data, even though $I(\nu, t, d, \theta)$ is not a linear function of time.

After generating time and space-integrated simulated spectra for the four different targets we can extract an 'integrated opacity' to compare with the experimental data. Furthermore, we can compare these values with the maximum instantaneous opacity at each photon energy that was observed in the simulation as the charge states evolved. In Fig. 3 we plot the energy-dependent opacity deduced from the experimental data alongside the opacity deduced from the space- and time-integrated intensities simulated by SCFLY. Good agreement is found over the majority of the spectral range (agreement for the 'cold' K-α line of the first state is not expected, as this is sensitive to how much FEL energy is in the far wings of the FEL focal spot). Also plotted is the ratio of the 'integrated opacity' extracted from the SCFLY simulations with the maximum instantaneous opacity calculated by SCFLY at that frequency. We find that at the peak of the K-α lines this ratio is reasonably consistent across the majority of charge states, varying from about 40% for line IV, up to 42% for line VI, and dropping to 35% for line X. Such consistency provides confidence that these time and space averaged opacity measurements are accurate representations of the maximum opacity to within of order $\pm 4\%$. We note that current discrepancies between measured and calculated opacities in systems considerably less dense than those here are many times larger than this [27].

That the 'integrated opacities' deduced from the experimental data are lower than the simulated maximum instantaneous opacity within the system by a roughly consistent amount can be understood by considering the evolution of the emitting and absorbing states. We find that the emitting and absorbing states rise and fall in time over a narrow ($\sim 20\,$fs) temporal window (see supplemental material). Thus the average opacity in the system is always lower than the maximum, and is roughly similar across the majority of the charge states.

We therefore find that the fitted 'integrated opacity' and emissivity plotted in Fig. 2b for line VI is thus constrained to conditions of temperature $T = 50 \pm 15\,$eV and electron density $n_e = 2.4 \pm 0.5 \times 10^{23}\,\mathrm{cm}^{-3}$ (the overall ion density remaining fixed at that of solid Mg, $4.31 \times 10^{22}\mathrm{cm}^{-3}$) whilst the spanned range of conditions extends up to $T = 120 \pm 25\,$eV, $n_e = 3.9 \pm 0.3 \times 10^{23}\,\mathrm{cm}^{-3}$ for the He-α line. The temperature eventually peaks around 180 eV at the end of the laser drive. As shown in the supplemental material, the densities and temperatures being probed by the emission from a particular charge state are relatively insensitive to the FEL pulse shape and fluence.

The slight discrepancies observed for the helium-like lines – where we find the deduced opacity is lower than expected – may be attributed to a lower final temperature than expected from SCFLY simulations for our spot parameters. We find that just by simply decreasing the laser intensity in our simulations by a factor of two gives the same evolution for the earlier charge states – which are still swept through in time, and still in LTE under the same temperature and density conditions [16], yielding the same opacity – but now reduces the opacity of the final charge states as, being last to be produced, their populations are the most sensitive to the total energy in the FEL pulse.

In conclusion, we have used LCLS to create hot Mg plasmas of varying thickness at exactly solid density, allowing the extraction of a measure of the LTE K-shell opacity in a solid-density plasma. We compare the values of the opacity extracted from fitting the data, using the uniform slab radiative transfer equation, with the opacity obtained in detailed predictive atomic kinetics simulations; such comparison shows that the opacity extracted from the fit has the physical meaning of a line

opacity integrated over a short time window, where both emitting and absorbing charge state for a given K-α line are populated. As such, it also corresponds to a certain fraction of the maximum opacity, which in our case is around 40% over a wide number of charge states. As the absorbing ions are ground state ions, which largely obey an LTE population distribution, the fit provides a good measure of solid-density LTE opacity. This method of extracting opacity from the variation of intensity with target thickness may complement methods based on absorption spectroscopy [27, 28]. Whilst the standard backlighting technique can be used to determine opacities for such longer-lived lower density plasmas [27], the technique presented here is well suited to the highly-transient plasmas at exactly solid density produced via irradiation with an FEL. We have also demonstrated the capability to produce well-characterised solid-density plasmas which are also measured to be optically thin, where the emission is produced before target disassembly (an Mg ion at 120 eV, would move around 2.5 nm in 50 fs, though the ions are likely to be far cooler than this as emission occurs on a time-scale short compared with temperature equilibration between electrons and ions [29]). Such plasmas could provide a platform for benchmark spectroscopic studies of dense plasmas, unhindered by opacity effects.

We wish to thank C. Spindloe and Scitech Precision Ltd. for manufacturing and characterising our target samples. Use of the Linac Coherent Light Source (LCLS), SLAC National Accelerator Laboratory, is supported by the U.S. Department of Energy, Office of Science, Office of Basic Energy Sciences under Contract No. DE-AC02-76SF00515. . T.R.P., O.C., P.H., and J.S.W. are grateful to the UK EPSRC for funding under grants EP/L000849/1, EP/H035877/1 and EP/P015794/1. S.M.V. is grateful to the Royal Society for support. T.B., J.Ch., V.H., L.J., and V.V. appreciate financial support from the Czech Ministry of Education (LG15013 and CZ.02.1.01 /0.0/0.0/16-013/0001552 - ERDF) and Czech Science Foundation (17-05167S).

* justin.wark@physics.ox.ac.uk

[1] F. J. Rogers and C. A. Iglesias, Science **263**, 50 (1994).
[2] T. Guillot, Science **286**, 72 (1999).
[3] J. D. Lindl *et al.*, Physics of Plasmas **11**, 339 (2004).
[4] S. X. Hu, B. Militzer, V. N. Goncharov, and S. Skupsky, Phys. Rev. Lett. **104**, 235003 (2010).
[5] K. Widmann, T. Ao, M. E. Foord, D. F. Price, A. D. Ellis, P. T. Springer, and A. Ng, Phys. Rev. Lett. **92**, 125002 (2004).
[6] Y. Ping, D. Hanson, I. Koslow, T. Ogitsu, D. Prendergast, E. Schwegler, G. Collins, and A. Ng, Physics of Plasmas **15**, 056303 (2008).
[7] Y. Ping *et al.*, High Energy Density Physics **6**, 246 (2010), {ICHED} 2009 - 2nd International Conference on High Energy Density Physics.
[8] P. K. Patel *et al.*, Phys. Rev. Lett. **91**, 125004 (2003).
[9] R. A. Snavely *et al.*, Physics of Plasmas **14**, 092703 (2007).
[10] W. Bang *et al.*, Scientific Reports **5**, 14318 EP (2015).
[11] P. Emma *et al.*, Nat Photon **4**, 641 (2010).
[12] S. M. Vinko *et al.*, Nature **482**, 59 (2012).
[13] O. Ciricosta *et al.*, Physical Review Letters **109**, 065002 (2012).
[14] A. Lévy *et al.*, Physics of Plasmas **22**, 030703 (2015).
[15] S. M. Vinko *et al.*, Nat Commun **6** (2015).
[16] O. Ciricosta, S. M. Vinko, H.-K. Chung, C. Jackson, R. W. Lee, T. R. Preston, D. S. Rackstraw, and J. S. Wark, Physics of Plasmas **022707** (2016), 10.1063/1.4942540.
[17] T. Holstein, Phys. Rev. **72**, 1212 (1947).
[18] G. Phillips, J. Wark, F. Kerr, S. Rose, and R. Lee, High Energy Density Physics **4**, 18 (2008).
[19] D. Rackstraw *et al.*, High Energy Density Physics **11**, 59 (2014).
[20] W. F. Schlotter *et al.*, Review of Scientific Instruments **83**, 043107 (2012).
[21] L. Young, E. P. Kanter, B. Krässig, Y. Li, a. M. March, S. T. Pratt, R. Santra, S. H. Southworth, N. Rohringer, L. F. DiMauro, G. Doumy, C. a. Roedig, N. Berrah, L. Fang, M. Hoener, P. H. Bucksbaum, J. P. Cryan, S. Ghimire, J. M. Glownia, D. a. Reis, J. D. Bozek, C. Bostedt, and M. Messerschmidt, Nature **466**, 56 (2010).
[22] O. Ciricosta, H.-K. Chung, R. W. Lee, and J. S. Wark, High Energy Density Physics **7**, 111 (2011).
[23] S. Düsterer, P. Radcliffe, C. Bostedt, J. Bozek, A. L. Cavalieri, R. Coffee, J. T. Costello, D. Cubaynes, L. F. DiMauro, Y. Ding, G. Doumy, F. Grüner, W. Helml, W. Schweinberger, R. Kienberger, A. R. Maier, M. Messerschmidt, V. Richardson, C. Roedig, T. Tschentscher, and M. Meyer, New Journal of Physics **13**, 093024 (2011).
[24] J. Chalupský *et al.*, Opt. Express **18**, 27836 (2010).
[25] A. G. de la Varga, P. Velarde, F. de Gaufridy, D. Portillo, M. Cotelo, A. Barbas, A. González, and P. Zeitoun, High Energy Density Physics **9**, 542 (2013).
[26] H.-K. Chung, M. H. Chen, and R. W. Lee, High Energy Density Physics **3**, 57 (2007).
[27] J. E. Bailey *et al.*, Nature **517**, 56 (2015).
[28] D. S. Rackstraw, O. Ciricosta, S. M. Vinko, B. Barbrel, T. Burian, J. Chalupský, B. I. Cho, H.-K. Chung, G. L. Dakovski, K. Engelhorn, V. Hájková, P. Heimann, M. Holmes, L. Juha, J. Krzywinski, R. W. Lee, S. Toleikis, J. J. Turner, U. Zastrau, and J. S. Wark, Physical Review Letters **114**, 015003 (2015).
[29] Z. Lin, L. V. Zhigilei, and V. Celli, Physical Review B - Condensed Matter and Materials Physics **77**, 1 (2008).